Detection and characterization of glaucoma-like canine retinal tissues using Raman spectroscopy

Qi Wang
Sinisa D. Grozdanic
Matthew M. Harper
Karl Hamouche
Nicholas Hamouche
Helga Kecova
Tatjana Lazic
Elena Hernandez-Merino
Chenxu Yu

Detection and characterization of glaucoma-like canine retinal tissues using Raman spectroscopy

Qi Wang,[a] Sinisa D. Grozdanic,[b] Matthew M. Harper,[b] Karl Hamouche,[a] Nicholas Hamouche,[c] Helga Kecova,[b] Tatjana Lazic,[b] Elena Hernandez-Merino,[b] and Chenxu Yu[a]

[a]Iowa State University, Department of Agricultural and Biosystems Engineering, Ames, Iowa 50011
[b]US Veterans Affairs Center for the Prevention and Treatment of Visual Loss, 601 HWY 6 West, Iowa City, Iowa 52246
[c]MacFarland Clinic Eye Center, 1128 Duff Avenue, Ames, Iowa 50011

Abstract. Early detection of pathological changes and progression in glaucoma and other neuroretinal diseases remains a great challenge and is critical to reduce permanent structural and functional retina and optic nerve damage. Raman spectroscopy is a sensitive technique that provides rapid biochemical characterization of tissues in a nondestructive and noninvasive fashion. In this study, spectroscopic analysis was conducted on the retinal tissues of seven beagles with acute elevation of intraocular pressure (AEIOP), six beagles with compressive optic neuropathy (CON), and five healthy beagles. Spectroscopic markers were identified associated with the different neuropathic conditions. Furthermore, the Raman spectra were subjected to multivariate discriminate analysis to classify independent tissue samples into diseased/healthy categories. The multivariate discriminant model yielded an average optimal classification accuracy of 72.6% for AEIOP and 63.4% for CON with 20 principal components being used that accounted for 87% of the total variance in the data set. A strong correlation ($R^2 > 0.92$) was observed between pattern electroretinography characteristics of AEIOP dogs and Raman separation distance that measures the separation of spectra of diseased tissues from normal tissues; however, the underlining mechanism of this correlation remains to be understood. Since AEIOP mimics the pathological symptoms of acute/early-stage glaucoma, it was demonstrated that Raman spectroscopic screening has the potential to become a powerful tool for the detection and characterization of early-stage disease. © 2013 Society of Photo-Optical Instrumentation Engineers (SPIE) [DOI: 10.1117/1.JBO.18.6.067008]

Keywords: glaucoma; early stage; acute elevation of intraocular pressure; compressive optic neuropathy; Raman spectroscopy; multivariate discriminate analysis; support vector machine; detection.

Paper 12683RR received Oct. 16, 2012; revised manuscript received May 29, 2013; accepted for publication May 30, 2013; published online Jun. 26, 2013.

1 Introduction

Glaucoma is a slowly progressive, chronic optic neuropathy that is characterized by retinal ganglion cell (RGC) death with subsequent loss of optic nerve axons and decrements in visual function. Glaucoma is diagnosed clinically by means of functional and structural analysis of the retina and optic nerve. After an initial diagnosis, these tests need to be repeated at regular intervals to assess the progress of the disease and any treatment effect. Unfortunately, a significant loss of retinal cells can occur before any of the current tests show an abnormality. Namely, between 25% and 35% of the RGCs could be lost before any visual field defect is detectable.[1] The detection of progressive changes in glaucoma can also be demanding, requiring multiple testing sessions over a prolonged period of time. Hence, a critical gap exists to develop clinical tests that could aid in the early diagnosis and monitoring of glaucoma.

Raman spectroscopy measures the inelastic scattering of laser light by biomolecules in tissue samples and can be used to predict the general biochemical composition of biological samples.[2] As such, it can be used to provide rapid characterization of healthy versus diseased tissues in a nondestructive and noninvasive fashion. In recent years, the technique has been applied to characterize various biological samples, including mineralized tissue such as bone and teeth,[3,4] skin,[5] brain,[6] the gastrointestinal tract,[7] mouth,[8,9] blood vessels,[10] and breast.[11] In ophthalmology, Raman spectroscopy has been used to determine carotenoid pigment levels in human retina,[12,13] altered vitreous molecules such as glycated collagen in diabetic vitreoretinopathy,[14] and the distribution of cholesterol in a rat eye lens,[15] as well as to detect glutamate in the vitreous of porcine eyes in an *ex vivo* experiment.[16]

Raman spectroscopy provides rapid characterization of the chemical composition and molecular structures in cells and tissues. Diseases and other pathological anomalies lead to chemical and structural changes at the molecular level in tissues that are reflected in their Raman spectra before the appearance of clinical symptoms. These spectral changes can be used as sensitive, phenotypic markers of disease[17] and could potentially lead to early disease diagnosis before clinical symptoms are apparent. Once Raman spectra are acquired, mathematical classification techniques are utilized to differentiate the spectral signatures of diseased and normal tissues. In our previous study, Raman spectroscopic screening was utilized to detect glaucomatous changes in retinal tissue with high specificity.[18] The specimens analyzed in that study were obtained from canine retinas with severe vision loss due to advanced hereditary angle-closure glaucoma. The physiological and biochemical retinal changes were quite significant in comparison to the healthy

Address all correspondence to: Chenxu Yu, Iowa State University, Department of Agricultural and Biosystems Engineering, Ames, Iowa 50011. Tel: 515-294-4554; Fax: 515-294-4250; E-mail: chenxuyu@iastate.edu

controls. It remains to be seen whether Raman spectroscopic screening can be used to detect glaucomatous changes at earlier stages of the disease in an animal model lacking any genetic predisposition for ocular pathology.

In order to better understand glaucomatous changes that occur at an early stage of glaucoma, it is essential to use animal models that recapitulate the development of the disease that is characterized by a progressive loss of RGC function. Elevated intraocular pressure (IOP) is considered a primary risk factor for the progression of glaucomatous neuropathy[19,20] and remains the etiological factor toward which all current therapeutic efforts are directed. Acute elevation of intraocular pressure (AEIOP) induces deformation of the lamina cribrosa and anterior scleral canal wall and underlies the onset of optic nerve head surface hypercompliance that is typically associated with an early stage of glaucoma.[21] Compressive optic neuropathy (CON) occurs when lesions appear along the optic nerve, which induces damage to the optic nerve and a progressive loss of visual function and structure.[22] Due to the similar size of the human and canine eye, functional and structural data can be acquired using instrumentation identical to that which is used in human patients.[23,24] In this study, retinal tissues from canine models of AEIOP and CON were compared to healthy control samples using Raman spectroscopy.

The primary purpose of this study was to explore the potential of using Raman spectroscopy for characterization of glaucoma-like spectroscopic signatures at an early stage of retinal damage to identify spectroscopic markers in the eyes and to classify methods to effectively differentiate early-stage glaucoma-like tissues and healthy tissues.

2 Materials and Methods

2.1 AEIOP in Beagles

Laboratory beagles were anesthetized with 2.5% halothane and a mixture of nitrous oxide and oxygen (30:70 ratio). Body temperature was maintained using a heating pad (T/Pump® Professional, Gaymar Industries Inc., Buffalo, NY). The pupils were dilated with topical 10% phenylephrine hydrochloride (Ak-dilate™, Akorn Inc., Buffalo Grove, IL) and 1% tropicamide (Tropicamide, Falcon Pharmaceuticals, Fort Worth, TX). Prior to anterior chamber cannulation, the eye was surgically prepped and a drop of 0.5% propracaine hydrochloride (Falcon Pharmaceuticals) was instilled. The anterior chamber was then cannulated with a 25-gauge needle connected to a reservoir containing 0.9% NaCl. The IOP in experimental eyes was controlled by adjusting the height of the reservoir to maintain a level of systolic blood pressure for 60 min. The systolic blood pressure was evaluated with an ultrasonic Doppler flow detector (Model 811-L, Parks Medical Electronics Inc., Las Vegas, NV) every 5 min. The average elevation of IOP was between 100 and 160 mmHg. After 60 min, the bottle was lowered and the needle was subsequently removed from the anterior chamber, and topical antibiotic ointment (Vetropolycin, Pharmaderm Inc., Melville, NY) was applied on the cornea. Postoperative treatment included one dose of hydromorphone HCl (0.1 mg/kg, Dilaudid, Abbott Laboratories, Lake Forest, IL) subcutaneously and application of topical antibiotic ointment to the operated eye twice daily for 2 days.[25]

2.2 Dog Model for CON

CON was induced in laboratory beagles by surgical implantation of custom-made silicone reservoir (Nagor LTD, Isle of Man, United Kingdom) into the left orbit. Animals were premedicated with intramuscular hydromorphone hydrochloride (0.1 mg/kg; Dilaudid®, Hospira, Inc., Lake Forest, IL) and acepromazine maleate (0.01 mg/kg, Vedco, Saint Joseph, MO). Anesthesia was induced with intravenous administration of propofol (3 to 5 mg/kg, Schering Plough Animal Health, Ethicon, NE) and maintained with 1.5% to 2.5% halothane (Halocarbon Laboratories, River Edge, NJ) in a mixture of 1:1 oxygen and nitrous oxide. Body temperature was maintained using a heating pad and a heating blanket (Bair Hugger®, Arizant Healthcare Inc., Eden Prairie, MN). Systolic, mean, and diastolic blood pressures were recorded with oscillometric arterial blood pressure monitor (Cardell Veterinary Monitor, Model 9401, Paragon Medical Supply, Coral Springs, FL) every 5 min and maintained in physiological levels with constant intravenous drip of lactated Ringer's solution (10 mL/kg for the first hour, 5 mL/kg after) during the orbital implant surgery and subsequent recordings. Heart rate, hemoglobin saturation, respiratory rate, expired CO_2, end-tidal CO_2, and end-tidal concentration of halothane were constantly monitored (Datascope Multinex Plus anesthesia monitor, Absolute Medical Equipment, New York, NY). After induction of anesthesia, the area around the left orbit and left side of the head was clipped and prepared for aseptic surgical procedure. Intravenous cefazolin (22 mg/kg; Cefazolin, Sandoz Inc., Princeton, NJ) was administered on a prophylactic basis, and the same dose was repeated every 2 h throughout the procedure.

With the animals in sternal recumbence, a skin incision was made above the left eye in the area of orbital ligament. The palpebral nerve was identified and, where necessary, retracted with sterile umbilical tape to avoid its damage during the procedure. The orbital ligament was incised lengthwise to enable access to the retrobulbar space. A Gelpi retractor was inserted into the incision to enable good visualization of the surgical site, and a custom-made inflatable silicone implant (Nagor) was introduced into the orbit, directly behind the eye. The injection port of the implant was passed through the incision in the orbital ligament and under the skin of the forehead into the occipital area, where it was fixed to the muscle fascia with absorbable monofilament suture (PDS 3-0, Ethicon). Surgical incisions were closed routinely. Postoperative analgesia and inflammation control were maintained with hydromorphone hydrochloride (0.1 mg/kg body weight) every 6 to 8 h (as needed) for 3 days and carprofen (4.4 mg/kg body weight) once daily for 7 days. The implant was inflated to a pressure that gave a complete optic nerve perfusion deficit as measured using fluorescein angiography. The device was then deflated until fluorescein was observed in the retina.

2.3 Animals and Tissue Collection

All animal studies were conducted in accordance with the Association for Research in Vision and Ophthalmology Statement for Use of Animals in Ophthalmic and Vision Research, and procedures were approved by the Iowa State University Committee on Animal Care. Eyes were collected from seven beagles with AEIOP and six beagles with CON for 24 h were used for Raman spectroscopic investigation. Additionally, eyes from five adult healthy beagles 6 months of age were used as controls. All control animals underwent ocular examination (slit-lamp biomicroscopy, IOP evaluation, indirect ophthalmoscopy, and gonioscopy) to rule out the possible presence of ocular disease before inclusion in the study. Eyes

were surgically removed from the beagles after euthanasia. They were fixed in 10% buffered paraformaldehyde for 24 h, rinsed, and paraffin embedded. Twenty-micron-thick retinal sections were made and placed on gold–aluminum coated histology slides for the purposes of Raman imaging. Raman spectra were acquired from the fixed tissue sections using a Raman microscope with 10× objective, with a laser spot size of ~50 μm diameter.

2.4 Acquisition of Raman Spectra from Retinal Tissues

In this study, Raman measurements were performed using a DXR Dispersive Raman Microscope (Thermo Scientific, Inc., Madison, WI) with 780 nm, 14 mW excitation laser with a charge-coupled device (CCD) camera and 50-μm pinhole in ambient temperature. Raman spectra were collected with 99 s exposure time from 600 to 2000 cm^{-1} at a resolution of 1 cm^{-1} (full-range grading).

2.5 Spectral Data Processing

The acquired Raman spectra were preprocessed to remove artifacts caused by background fluorescence and intensity fluctuations.[17,26] Using near-infrared excitation (780 nm) radically reduces the observance of sample autofluorescence. To further reduce the remaining fluorescence, a polynomial background subtraction method was implemented.[27] Another challenge in spectral preprocessing is to capture important patterns in the spectra while removing noise or other fine-scale structures. The 10-point moving average method was used in this study to smooth the spectra. Finally, all spectra were area normalized for intensity consistency at the region between 600 and 2000 cm^{-1}. All data processing was conducted using R, a widely used open-source language and software tool for statistical computing and graphics downloaded freely from the Internet (www.>r-project.org).

2.6 Principal Component Analysis

In Raman spectra, each wave number represents a dimension or variable. Commonly, data in one Raman spectrum contains thousands of dimensions, which makes statistical analysis much more challenging. For discriminant analysis, as the (number of) dimensions of the data becomes large, the limitation on the capability of detecting distinguishable classes becomes severe.[28] Due to the fact that most statistical methods are based on optimization criteria, it is advisable to reduce the dimension(s) of the problem, which results in decreasing computational costs and increasing probability of finding the best model representing the data. For this purpose, often a principal component regression is utilized:

$$Y = L \times S^{\mathrm{T}} + E.$$

In the equation above, Y is the matrix of spectra, S is the score matrix, L is the matrix of loadings, and E is the error matrix. The data are compressed into principal component (PC) scores.

All spectra were polynomial baseline corrected, smoothed using moving average algorithms, and area normalized at the region between 600 and 2000 cm^{-1} before principal component regression was utilized. Ten to forty PCs (which account for at least 90% of total variance in the data) were selected from thousands of dimensional hyperspectral data as inputs for multivariate discriminant classification model.

For each dog in AEIOP and CON groups, the calculated PC spectra form a cluster. The average intracluster Euclidean distances in the multidimensional PC space (one dimension represents one principal component for our data) are calculated between each diseased dog and the control group (i.e., all spectra from the control dogs). Our hypothesis is that more distinguishable spectroscopic signatures between diseased dogs and the control group will translate into a higher separation distance in the multidimensional PC space. Hence, the calculated average distance may serve as a base for a disease score system that predicts the severity of the disease conditions. This hypothesis was checked against AEIOP, CON, and late-stage close-angle glaucoma, with mixed results. More work is needed to further refine the disease score system.

## 2.7 Cross-Validation, Independent Validation, and Discriminant Modeling

Cross-validation is a technique for assessing how the results of a statistical analysis will generalize to an independent dataset.[29] One round of cross-validation involves partitioning a sample of data into complementary subsets, performing the analysis on one subset (called the training set), and validating the analysis on the other subset (called the validation set or testing set). To reduce variability, multiple rounds of cross-validation are performed using different partitions, and the validation results are averaged over the rounds.

One inherent drawback of cross-validation comes from the fact that the validation set and the training set are indeed spectra measured from the same batch of samples (i.e., dogs). The high prediction accuracy reported from cross-validated discriminant models can be biased. In this study, to further confirm that Raman spectroscopic data can yield enough information that distinguishes diseased tissues from normal ones, even at an early stage of the disease, we tested the discriminant model by independent validation. In this approach, spectra from two beagles in each group were randomly selected as validation datasets that were excluded from the training pool used to create the support vector machine (SVM) classification models. Ten repetitions were conducted. Twenty PCs were used to develop the discriminant model. The validation set only contains spectral data that were acquired from an independent set of samples (i.e., dogs), with no overlap with the sample pool from which the spectral data for the training of the discriminant model were acquired.

In general, all spectra were baseline corrected, smoothed to reduce the baseline variability, and normalized using R before classification analysis. SVM based on R packages "e1071"[30] with folded cross-validation was utilized as the discriminant classification modeling technique.

2.8 Pattern Electroretinography Characterization of the Disease Status of AEIOP Dogs

The pattern electroretinogram (pERG), which measures the retinal response evoked by viewing a temporally alternating pattern, is important in providing information about RGC function. With appropriate paradigms, pERG is objectively correlated with the overall RGC status.[31] The P50 and the N95 components were affected rather similarly by glaucoma in pERGs. In this
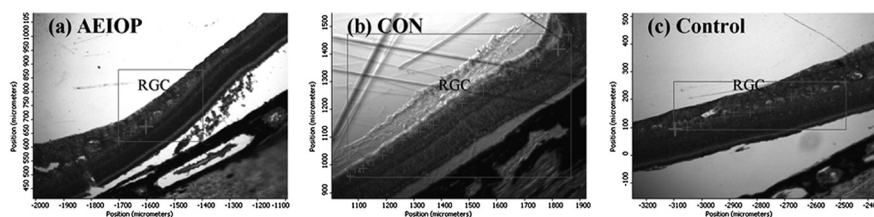
Fig. 1 Optic images of retinal tissue sections from a AEIOP beagle (a), a CON beagle (b), and a healthy beagle (c) on gold-coated slides (RGC-retinal ganglion cell layer).

study, pERG was performed to evaluate the damage induced by elevated IOP to RGCs in the AEIOP dogs. pERGP50-N95 amplitude and P50op/P50ctrl ratio were obtained following ISCEV standard.[32]

3 Results and Discussion

3.1 Spectroscopic Difference Between the RGCs of AEIOP, CON, and Healthy Beagles

The optical images of the retinal tissue sections of AEIOP beagle, CON beagle, and healthy beagle are shown in Fig. 1. The layers of RGCs were identified under the microscope, as shown in the figures. To compare the biochemical changes represented by the Raman spectroscopic signatures, we measured Raman spectra from 133 RGCs from five healthy beagles with normal vision, 114 RGCs from seven AEIOP beagles, and 160 RGCs from six CON beagles. The difference spectra were acquired by subtracting the average spectrum of control (healthy beagle) from the diseased (AEIOP or CON) average spectra (Fig. 2).

The wave number and intensity changes in the Raman bands are indicative of changes in the secondary structure and variations of intracellular proteins as well as local cellular

environments. Looking at the actual and difference spectral graphs between AEIOP, CON, and normal beagles (Fig. 2), we noted hikes corresponding to the Amide III (1252 cm^{-1}) and Amide I (1656 cm^{-1}) peaks in both conditions. The differences in these regions between AEIOP, CON, and normal dogs are all over three times of the standard deviations (std) within each group (i.e., stds of pooled AEIOP spectra, CON spectra, and normal spectra); hence, they represent the true spectral changes between groups. While the total protein concentration indicated by the Amide III peak[31] seems to be increased in both conditions, suggesting an elevated protein synthesis in the RGCs, there are significant differences in the Raman bands of various amino acids at 800 to 1200 cm^{-1} in AEIOP/CON RGCs compared to healthy RGCs. This suggests that either different genes are being expressed leading to a different protein composition in each of the two conditions or gene expression levels are different in each of the two conditions. Both represent changes at a molecular level inside the RGCs. The Amide I peak, on the other hand, may be caused by different concentrations of cholesterol, ceramide, and unsaturated fatty acids which have cis C=C Raman bands at 1650 cm^{-1}. Also, the difference spectra reveal that, in general, the changes in AEIOP RGCs are more
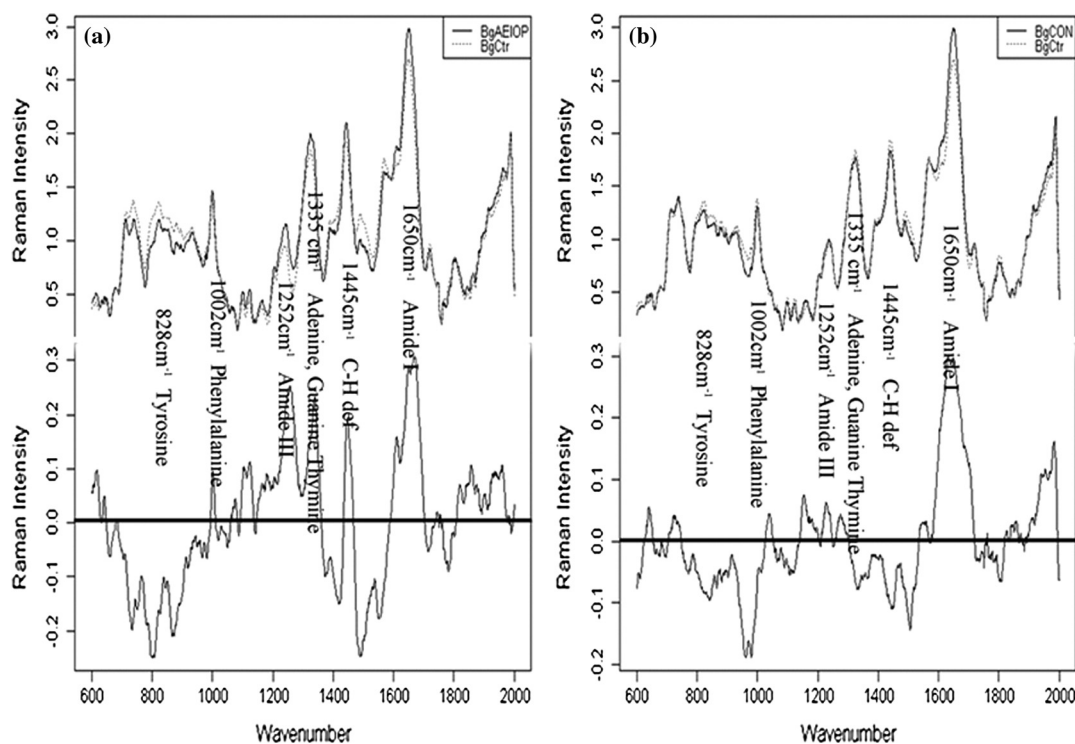
Fig. 2 (a), Average spectrum of RGCs from AEIOP beagles and healthy beagles, and the difference spectrum between them. (b), Average spectrum of RGCs from CON beagles and healthy beagles, and the difference spectrum between them. Difference spectra were acquired by subtracting the average spectrum of control (healthy) from the diseased (AEIOP or CON) dogs.
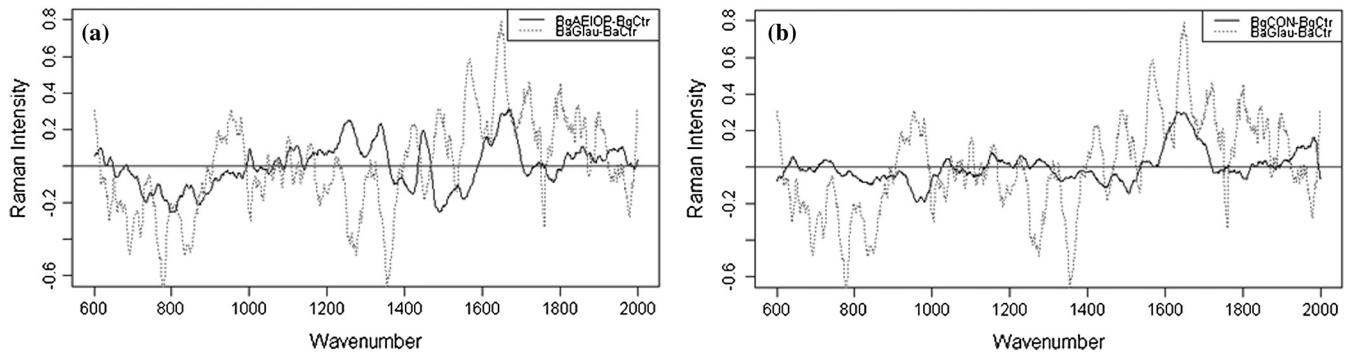
Fig. 3 Comparison between spectroscopic markers for AEIOP, CON, and late-stage close-angle glaucoma. (a), AEIOP markers versus glaucoma markers. (b), CON markers versus glaucoma markers.

significant than those of CON RGCs. This is consistent with the fact that AEIOP has a more direct and probably more generalized impact on the RGCs than CONs.

3.2 Spectroscopic Differences Between AEIOP/CON Beagles and Advanced Glaucoma in Basset Hounds (BaGlau)

Another interesting comparison is between AEIOP, which mimics acute/early-stage glaucoma, CON, which is a different pathological process although sharing some clinical findings with glaucoma, and BaGlau, which probably resembles later-stage glaucoma in our scenario. The late-stage glaucoma spectra were acquired from diseased/control basset hounds reported previously.[2] Although the different breeds may introduce additional variations to the spectral data, it has been shown in our previous work that the diseased/healthy conditions are still the determining factor that dictates the spectral signatures.[2]

In Fig. 3, we have shown the difference spectra of AEIOP, CON, and late-stage glaucoma (BaGlau). It is clear that the spectroscopic changes in the RGCs associated with late-stage glaucoma are more significant than those of the AEIOP/CON RGCs (the intensity changes associated with the disease conditions are three to four times higher in late-stage glaucoma comparing to those of AEIOP/CON). At a later stage of disease, most RGCs are dead and the remaining RGCs are biochemically different from healthy living RGCs, which may explain the more significant spectroscopic changes. Interestingly, no change is observed for the Amide III peak (1225 cm^{-1}) in late-stage glaucoma RGCs, suggesting no significant change in total protein concentration. This suggests that at an early stage of the disease, the RGCs behave differently in terms of protein synthesis. As we know, the spectra reflect the biochemical composition of the cellular milieu at the time of the test. The composition of the milieu depends on the balance between the production and clearance of the "apoptotic" proteins and other molecules. The qualitative differences between the spectra of AEIOP/CON and "late" glaucoma may suggest that in late-stage glaucoma, there are more significant changes in the protein synthesis pattern, and the cumulative accumulation of apoptotic proteins and other molecules in the retina might be the reason for the observed spectroscopic differences. The summation of these changes may potentially be used as spectroscopic markers for the *in vivo* diagnosis of glaucoma.

Another interesting observation is the overlap between the AEIOP spectral markers and those of late-stage glaucoma in the amino acid fingerprinting regions (700 to 1200 cm^{-1})

and the lack of such an overlap with the CON spectral markers. Since AEIOP shares many pathophysiologic features of acute glaucoma, it is reasonable to assume that spectral markers for AEIOP may be good for early-stage glaucoma and function as indicators of risk and susceptibility to the disease.

3.3 Discriminant Classification Using SVM

SVM using Raman spectroscopic binary barcodes was utilized to generate discriminant classification models to classify a measured spectrum from a retinal tissue sample into groups of two categories (AEIOP and healthy, CON and healthy, AEIOP and CON). One hundred and thirty-three spectra measured from the control group (five healthy beagles), 114 spectra measured from the seven AEIOP beagles, and 160 spectra measured from six CON beagles were used for the discriminant analysis. To construct the discriminant model, the spectra from each category were randomly assigned into 10 blocks, and 8 blocks were randomly chosen to train the SVM model (the detail of the SVM model was reported elsewhere),[2] whereas the remaining two blocks were used as validation testing sets. This training-validation cycle was repeated 10 times; each time new blocks were constructed through random assignment. The average classification accuracy was subsequently calculated.

Table 1 shows the classification accuracy for AEIOP/control and CON/control with different numbers of PCs being used in the discriminant models. At 20 PCs, with 87% of the total variance accounted for, the classification accuracies for both AEIOP and CON reached their optimal values (81.2% and 73.3%, respectively). The classification accuracies for the AEIOP samples are consistently better than those for the CON samples, suggesting that the Raman spectral measurements of the RGCs provided a better characterization of the AEIOP physiological
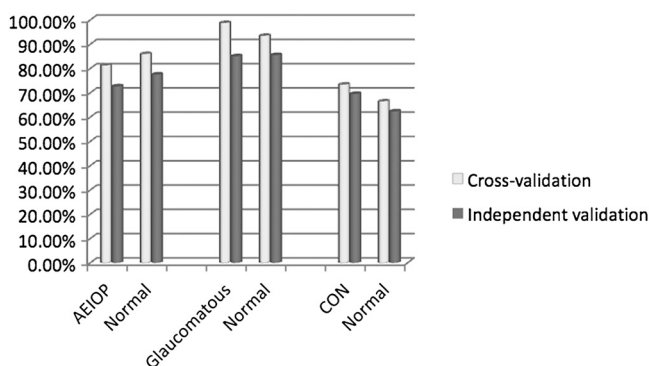
Table 1 Classification accuracy (%) with different PCs used in the discriminant modeling.

| No. of PCs (% of variance)		40 (92%)	20 (87%)	10 (70%)
AEIOP versus normal	AEIOP	74.4	81.2	78.7
	Normal	89.5	85.9	60.2
CON versus normal	CON	71.6	73.3	65.5
	Normal	69.7	66.4	61.6

conditions than those of CON cases. To better detect changes associated with CON, different cell types, or a combination of cell types (other than RGCs) in the retinal tissue may need to be characterized.

It is well known that classification models tend to yield high accuracy when the training data and the validation data are acquired from the same sources. For the spectroscopic screening to become a viable clinical tool, it needs to classify independent samples (not in the training pool) with high accuracy. In this study, we investigated the classification testing with independent validation. The average classification accuracy was then calculated to evaluate the performance of the classification models (Fig. 4). As expected, the results confirm that an independent validation dataset does lead to a reduction in prediction accuracy. When independent samples (i.e., dogs) are used for the validation tests, individual differences between the validating samples and the samples in the training pool that are not due to diseases would contribute to the discriminant calculation and result in a less accurate prediction. For AEIOP, the classification accuracy went from 82.1% to 72.6%, and for CON, it went from 73.3% to 63.4%. Since in clinical settings, a new patient will certainly be an "independent" sample that is not currently included in the training pool from which the discriminant model is developed, it is more relevant from a potential application standpoint that the independent validation should be conducted.

Another observation is that the prediction accuracies for AEIOP and CON are both lower than that for the late-stage glaucoma cases (for late-stage glaucoma, an average accuracy of 97.6% was reported),[2] without taking into account the effect of independent validation. RGCs from retinal tissues of late-stage glaucoma dogs are expected to differ more significantly from those of healthy dogs. It was further confirmed by calculating the Euclidean distances for Raman spectra from RGCs between group CON and group control, group AEIOP and group control, group late-stage glaucomatous BaGlau and group control in the multidimensional PC space. Longer distance suggests greater separation between the groups. As shown in Fig. 5, the distance between group late-stage glaucomatous and control is the highest, suggesting that most of the significant differences were observed between the late-stage glaucomatous group and the control group. It also shows that
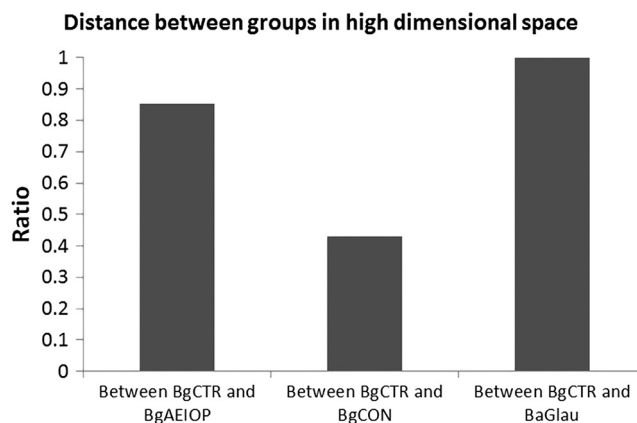
Fig. 5 Distance between groups in high-dimensional space. The Euclidean distances for Raman spectra from RGCs between group CON and group control, group AEIOP and group control, group late-stage glaucomatous BaGlau and group control were calculated in 20-dimensional space (one principal component means one dimension). The distances were recalibrated by being divided by the distance between group BaGlau and group control.

the distance between the AEIOP group and the control group is larger than that between the CON group and the control group, which is consistent with the higher classification accuracy for AEIOP samples versus CON samples (82.1% versus 73.3%, respectively). The average independent prediction accuracy for AEIOP (72.6%) is a good indicator of the potential prediction accuracy for early-stage glaucoma, which is currently not effectively being diagnosed. In addition, this observation also suggests that AEIOP spectra exhibit more similarity to those of glaucomatous tissues, indicating that AEIOP is a good model to simulate early-stage glaucoma.

3.4 Limitations and Future Directions

An interesting observation is the apparent negative correlation between the Raman separation distance of diseased and control groups and the electrophysiological characteristics of the RGCs acquired by pattern electroretinography (pERGP). The separation distances between seven AEIOP dogs and the control group (used as Raman predictive score) were calculated. This distance measures the statistical separation between the control group and the AEIOP dogs. However, as shown in Table 2 and Fig. 6, the scores correlate strongly with the pERGP data in a negative fashion. Higher pERG amplitude or ratio suggests healthier RGCs; hence one would expect a shorter separation between the diseased dog and the control group. However, as shown in Table 2 and Fig. 6, an almost opposite trend is observed. Higher pERG readings are consistent with higher separation distances, with strong correlation indicated by the high R^2 values. Dog #2 has the highest pERG readings, and the largest Raman separation distance in multidimensional PC space as well. Moreover, a strong linear correlation could be established between the Raman separation distances and the pERG ratio between diseased and control dogs, but the pERG amplitude at P50 to N95 seems to correlate with the Raman separation distance in a logarithmic manner. More study is needed to explain this controversial result. Raman spectra measure the overall chemical compositional characteristics of the RGCs. The PC scores for different dogs with various disease conditions may vary in their contribution to the overall variance. The Raman

Fig. 4 Average classification accuracies for RGCs from SVM discriminant model to differentiate healthy tissues from AEIOP tissues, CON tissues, and late-stage glaucomatous tissues; validated through cross-validation dataset (training and validation data from same sample pool), and independent validation dataset (training and validation data from same sample pool).

Table 2 Pattern electroretinography parameters and calculated Euclidean distance between individual AEIOP beagles to control beagles in 20 PC space.

	AEIOP1	AEIOP2	AEIOP3	AEIOP4	AEIOP5	AEIOP6	AEIOP7
pERGP50-N95	2.81	12.4	1.07	2.03	2.51	2.36	0.52
P50op/P50 ctrl (%)	46	89	15.4	44.6	60.19	50.2	15.24
Distance	24.405	50.7	8.235	23.315	31.35	26.28	7.88

separation distance in PC space, therefore, may not be a direct indicator to determine the loss of function in RGCs measured by pERGP. Further characterization of the chemical compositional changes in RGCs associated with the change in pERGP readings is needed for direct identification of Raman spectral peaks that are affected and vice versa. The pERGP measurements are conducted with living tissues, whereas the Raman spectra were measured from fixed tissue samples, which may also complicate the correlations between the pERG readings and the Raman separation distances. Nonetheless, the strong correlation between the pERG readings and the Raman separation distances still suggested that Raman spectra of diseased retinal tissues do capture important signatures that are correlated to the onset and progression of glaucoma-like disease such as AEIOP.

In this study, with the maximum laser exposure time at 99 s, the threshold limit value (TLV), which determines the maximum permissible energy exposure to the retina in an *in vivo* measurement, is 0.82 mW/cm^2. Our power density on sample was 140 mW/cm^2, significantly higher than the TLV. To utilize Raman spectroscopy for *in vivo* imaging, the laser power density on the retina has to be greatly reduced without sacrificing the spectral quality. A possible solution would be to utilize pulse laser with extreme short time-resolved detection (e.g., picoseconds to nanoseconds). With such short detection time (i.e., laser exposure time), background fluorescence is eliminated (shorter than the fluorescence lifetime so that fluorescence is not developed), and the signal-to-noise ratio of the Raman spectral measurement can be significantly improved, and much weaker Raman signals will become detectable.[32,33] Extremely short detection time also allows a much higher laser power to be applied without increasing the overall laser energy that the retina is exposed to.

Another limitation of our study is the fact that we are looking at an acute and a substantial loss of retinal tissue, particularly in the AEIOP animals. This is most likely resulting in more severe damage and dysfunctional RGCs in the retinal tissues than in the case of early-stage glaucoma. In a more typical clinical scenario in which a Raman system is hoped to help, open-angle glaucoma is a more chronic disease with a much smaller number of RGCs being lost at any particular time, leading to a less differentiable Raman spectral signal that needs to be distinguished from that of normal tissues.

4 Conclusion

In this study, we explore the potential of using Raman spectroscopy for early detection and characterization of glaucoma-like pathological anomalies. Spectroscopic markers related to changes in intracellular protein compositions associated with glaucoma-like anomalies of RGCs were identified. Classification accuracy (72.6%) was achieved to identify AEIOP, a close mimic of early-stage/acute glaucomatous damage, from independent canine retinal tissues. Potentially, Raman spectroscopy in combination with time-gated pulsed laser excitation can be utilized for *in vivo* Raman imaging of retina and provide early detection and diagnosis for glaucoma.
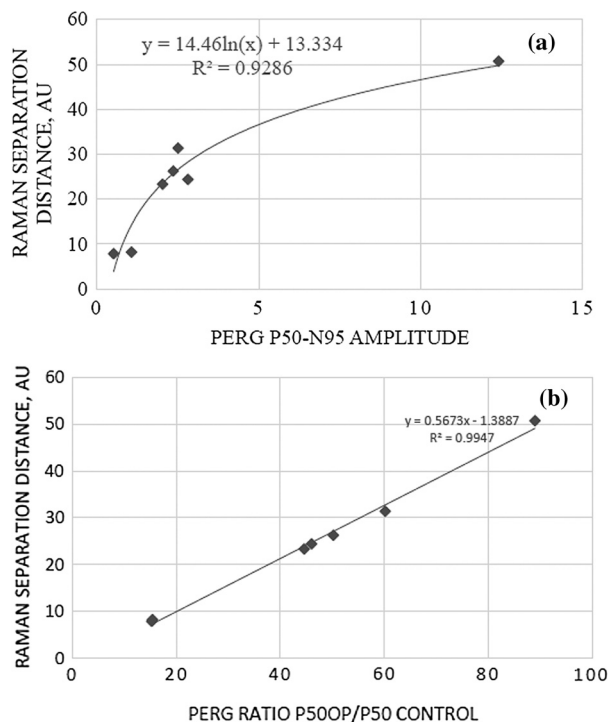
Fig. 6 Correlations between the pERG data and the Raman separation distance predictor for AEIOP dogs. (a), Correlation between pERG P50-N95 amplitude and Raman separation distance. (b), Correlation between pERG P50OP/P50 control ratio and Raman separation distance.

References

1. L. A. Kerrigan-Baumrind et al., "Number of ganglion cells in glaucoma eyes compared with threshold visual field tests in the same persons," *Invest. Ophthalmol. Visual Sci.* **41**(3), 741–748 (2000).
2. Q. Wang et al., "Exploring Raman spectroscopy for the evaluation of glaucomatous retinal changes," *J. Biomed. Opt.* **16**(10), 107006 (2011).
3. A. L. Boskey and R. Mendelsohn, "Infrared spectroscopic characterization of mineralized tissues," *Vib. Spectrosc.* **38**(1–2), 107–114 (2005).
4. A. C. T. Ko et al., "Detection of early dental caries using polarized Raman spectroscopy," *Opt. Express* **14**(1), 203–215 (2006).
5. L. Knudsen et al., "Natural variations and reproducibility of *in vivo* near infrared Fourier transform Raman spectroscopy of normal human skin," *J. Raman Spectrosc.* **33**(7), 574–579 (2002).
6. S. Koljenovi et al., "Tissue characterization using high wave number Raman spectroscopy," *J. Biomed. Opt.* **10**(3), 031116 (2005).
7. M. G. Shim et al., "*In vivo* near infrared Raman spectroscopy: demonstration of feasibility during clinical gastrointestinal endoscopy?," *Photochem. Photobiol.* **72**(1), 146–150 (2000).
8. T. C. B. Schut et al., "*In vivo* detection of dysplastic tissue by Raman spectroscopy," *Anal. Chem.* **72**(24), 6010–6018 (2000).
9. Z. Huang et al., "Raman spectroscopy in combination with background near infrared autofluorescence enhances the *in vivo* assessment of malignant tissues," *Photochem. Photobiol.* **81**(5), 1219–1226 (2005).
10. S. Van de Poll et al., "On-line detection of cholesterol and calcification by catheter based Raman spectroscopy in human atherosclerotic plaque *ex vivo*," *Heart* **89**(9), 1078–1082 (2003).
11. K. E. Shafer Peltier et al., "Raman microspectroscopic model of human breast tissue: implications for breast cancer diagnosis *in vivo*," *J. Raman Spectrosc.* **33**(7), 552–563 (2002).
12. W. Gellermann, "Raman imaging of human macular pigments," *Opt. Lett.* **27**(10), 833–835 (2002).
13. P. S. Bernstein et al., "Resonance Raman measurement of macular carotenoids in the living human eye," *Arch. Biochem. Biophys.* **430**(2), 163–169 (2004).
14. J. Sebag, "Seeing the invisible: the challenge of imaging vitreous," *J. Biomed. Opt.* **9**(1), 38–46 (2004).
15. N. M. Sijtsema et al., "Imaging with extrinsic Raman labels," *Appl. Spectrosc.* **50**(5), 545–551 (1996).
16. E. F. Kruger et al., "Detection of glutamate in the eye by Raman spectroscopy," *J. Biomed. Opt.* **8**(2), 167–172 (2003).
17. C. Krafft and V. Sergo, "Biomedical applications of Raman and infrared spectroscopy to diagnose tissues," *Spectroscopy* **20**(5), 195–218 (2006).
18. Q. Wang et al., "Exploring Raman spectroscopy for the evaluation of glaucomatous retinal changes," *J. Biomed. Opt.* **16**(10), 107006 (2011).
19. H. A. Quigley, "Neuronal death in glaucoma," *Prog. Retinal Eye Res.* **18**(1), 39–57 (1999).
20. J. C. Morrison, "Elevated intraocular pressure and optic nerve injury models in the rat," *J. Glaucoma* **14**(4), 315–317 (2005).
21. A. J. Bellezza et al., "Deformation of the lamina cribrosa and anterior scleral canal wall in early experimental glaucoma," *Invest. Ophthalmol. Visual Sci.* **44**(2), 623–637 (2003).
22. C. A. Girkin, "Compressive optic neuropathy," in *Neuro-ophthalmology: The Practical Guide*, pp. 217–221, Thieme Medical Publishers, Inc, New York, NY (2005).
23. K. Gelatt, "Animal models for glaucoma," *Invest. Ophthalmol. Visual Sci.* **16**(7), 592–596 (1977).
24. S. D. Grozdanic et al., "Functional and structural changes in a canine model of hereditary primary angle-closure glaucoma," *Invest. Ophthalmol. Visual Sci.* **51**(1), 255–263 (2010).
25. S. D. Grozdanic et al., "Recovery of canine retina and optic nerve function after acute elevation of intraocular pressure: implications for canine glaucoma treatment," *Vet. Ophthalmol.* **10**, 101–107 (2007).
26. J. Zhao et al., "Automated autofluorescence background subtraction algorithm for biomedical Raman spectroscopy," *Appl. Spectrosc.* **61**(11), 1225–1232 (2007).
27. L. O. Jimenez and D. A. Landgrebe, "Supervised classification in high-dimensional space: geometrical, statistical, and asymptotical properties of multivariate data," *IEEE Trans. Syst. Man Cybern. C Appl. Rev.* **28**(1), 39–54 (1998).
28. L. O. Jimenez and D. A. Landgrebe, "Supervised classification in high-dimensional space: Geometrical, statistical, and asymptotical properties of multivariate data," *IEEE Trans. Syst. Man Cybern. C Appl. Rev.* **28**(1), 39–54 (1998).
29. I. H. Witten and E. Frank, *Data Mining: Practical Machine Learning Tools and Techniques*, Morgan Kaufmann, Burlington, MA (2005).
30. A. Karatzoglou, D. Meyer, and K. Hornik, "Support vector machines in *R*," *J. Stat. Softw.* **15**(9), 1–27 (2006).
31. A. M. Herrero, "Raman spectroscopy for monitoring protein structure in muscle food systems," *Crit. Rev. Food Sci. Nutr.* **48**(6), 512–523 (2008).
32. T. Tahara and H. O. Hamaguchi, "Picosecond Raman spectroscopy using a streak camera," *Appl. Spectrosc.* **47**(4), 391–398 (1993).
33. P. Matousek et al., "Efficient rejection of fluorescence from Raman spectra using picosecond Kerr gating," *Appl. Spectrosc.* **53**(12), 1485–1489 (1999).